Low-voltage, megawatt free-electron lasers at a frequency near 300 GHz*

J. H. Booske, V. L. Granatstein, T. M. Antonsen, Jr., W. W. Destler, B. Levush, I. D. Mayergoyz, D. Radack, J. Rodgers, E. T. Rosenbury, Z. Segalov, and A. Serbeto

Laboratory for Plasma and Fusion Energy Studies
University of Maryland, College Park, MD 20742-3511

ABSTRACT

Design procedures and beam transport feasibility experiments are discussed for a novel, millimeter-wave free electron laser (FEL) concept employing short period magnetic undulators and a sheet electron beam. The advantages of this concept include: (1) lower beam voltage (~500 kV) compatible with thermionic Pierce gun technology and conventional power supplies (rather than electron accelerators), (2) a sheet electron beam geometry which enables high power operation without excessively high gun perveance, and (3) a streaming electron beam which is compatible with depressed collector beam energy recovery for enhancing overall system efficiency. Conceptual designs for pulsed and cw high power devices, and a cw low power device are presented.

1. INTRODUCTION

Development of high power space-borne radar systems capable of operating at wavelengths near one millimeter would be of great benefit to the communication and tracking tasks required of strategic defense. Compared with conventional, longer wavelength radars, superior target imaging resolution would be achievable. Millimeter-wavelength radar would also permit better penetration of an atmosphere filled with nuclear debris.

Of various high power millimeter wave generation devices studied in laboratories, only the free electron laser mechanism has demonstrated power in excess of 1 MW near the desired wavelength of 1 mm.[1] To date, however, these results have only been achieved using pulse line accelerators with pulselengths less than or equal to a few tens of nanoseconds. Radar applications would require sources at similar peak power and wavelength but with repetitive pulsing and pulselengths up to a microsecond. Furthermore, for deployment in space, the sources should be compact and lightweight; this requirement would presumably put a premium on high total system efficiency. There would also be a preference for lower voltage, and permitting the use of more compact conventional power supplies and modulators while obviating the need for electron accelerators.

At the University of Maryland, we are investigating the possibilities of a new free electron laser (FEL) configuration which is intended to decrease the voltage requirement while keeping output power large and achieving a high total system efficiency. First, a small period undulator (5 mm $< \ell_w <$ 10 mm) is used to reduce the beam voltage necessary for millimeter-wave FEL operation to approximately 500 keV. This reduction in beam voltage enables the utilization of low-emittance, conventional, thermionic cathode, Pierce electron guns.

Second, we employ the use of a sheet electron beam. For strong FEL interaction, all the electrons must be a small distance from the undulator magnet compared with the undulator period. For a small period undulator, this implies a very small dimension for the electron beam in at least one transverse dimension. To keep beam current and power large, we propose to make the beam large in the second transverse dimension. The sheet electron beam would typically have a thickness of 0.5-1.0 mm and a width of several centimeters.

Third, in order to increase overall FEL system efficiency, we propose the use of multistage depressed collectors to recover energy in the spent electron beam. The successful development of such collectors will reduce the voltage requirement of the modulator to about 100 kV, requiring only a very low current biasing supply with very low current at the 500 kV level. Thus, there is potential for developing 1 MW tubes at frequencies near 300 GHz, utilizing compact modulators and power supplies that are well within the present state-of-the-art, rather than electron accelerators.

A cross-sectional sketch of the sheet beam FEL is shown in Figure 1 together with a high

*Sponsored by SDIO/IST through a contract managed by the Harry Diamond Laboratory.

voltage bias supply (ϕ_{HV}) and a lower voltage supply (ϕ_{LV}), which carries the full beam current. In this paper, we describe design procedures and early progress in studying the feasibility of such an FEL. Section II describes design procedures, including scaling laws for self-consistent sheet beam FEL oscillators. Section III describes results of recent sheet beam propagation experiments. A summary of the status of our studies is presented in Section IV.

2. SHORT PERIOD UNDULATOR FEL OSCILLATOR DESIGN

2.1. Accessible frequencies

As mentioned above, to obtain undulator fields with sufficient strength for FEL interaction in short period planar undulators, one must utilize a narrow gap δ between the magnet pole pieces. In particular, our studies have found that a gap-to-period ratio $\delta/\ell_w \leq 0.5$ is necessary to obtain peak wiggler fields of several kilogauss.[1]

As a result of this restriction on undulator magnet separation, the interaction region will be bounded by thin, closely spaced (δ is on the order of one or two free space radiation wavelengths) conducting walls. Hence a calculation of the FEL operating frequency must account for waveguide dispersion

$$\omega^2 = \omega_{co}^2 + k_z^2 c^2, \tag{1}$$

as well as phase resonance

$$\omega \approx (k_w + k_z)\beta_z c. \tag{2}$$

Here, $k_w = 2\pi/\ell_w$ is the wiggler "wavenumber" and $\beta_z = v_z/c$ is the normalized axial velocity. The lowest order rectangular vacuum waveguide mode which has a resonant FEL interaction with the sheet electron beam is the TE_{01} mode.[2] For FEL operation with this mode, Equations (1) and (2) can be simultaneously solved for the resonant frequencies

$$\omega = \beta_z \gamma_z^2 \, k_w c\{1 \pm [\beta_z^2 - (\frac{1}{2\rho\gamma_z})^2]^{1/2}\}, \tag{3}$$

where $\gamma_z = [1 - \beta_z^2]^{-1/2}$ is the relativistic axial energy parameter, $\rho = b_{rf}/\ell_w$ is the ratio of the narrow transverse waveguide dimension b_{rf} to the wiggler period, and b_{rf} is related to the magnet gap spacing via the waveguide wall thickness t_{rf}:

$$b_{rf} = \delta - 2\, t_{rf}. \tag{4}$$

Nonzero beam density (i.e. collective) effects have not been included in Equation (3). Substituting Equation (4) into Equation (3) yields the plot of accessible resonant FEL frequencies versus beam voltage shown in Figure 2. The region above the solid line represents points for which $\delta > \ell_w/2$ (i.e., weak wiggler fields for a short period wiggler). Points below the solid line are accessible with the right combination of wiggler period and beam voltage. Thus, 150 to 300 GHz FELs with beam voltages of 500 kV require wiggler periods of 1.0 to 0.5 cm, respectively. Frequencies as high as 600 GHz may be accessible if 750 kV thermionic Pierce guns or undulators with $\ell_w < 0.5$ cm are found to be technologically feasible.

2.2. FEL oscillator equilibria calculations

To determine achievable FEL oscillator equilibria it is assumed that collective effects may be ignored and thus we start with Hamilton's equations for an axially streaming electron in the presence of a magnetostatic undulator and an electromagnetic radiation field:

$$\frac{dz}{dt} = \frac{\partial H}{\partial P_z} \tag{5a}$$

$$\frac{dP_z}{dt} = -\frac{\partial H}{\partial z} \tag{5b}$$

$$H = mc^2 \left[1 + \left(\frac{P_z}{mc}\right)^2 + \left(\frac{qA_x}{mc^2}\right)^2\right]^{1/2} \tag{5c}$$

$$A_x = A_w \cos(k_w z) + A_s \tag{5d}$$

In these equations, z is the electron's axial position, P_z is the conjugate canonical momentum, and A_x is the combined undulator (A_w) and radiation field (A_s) vector potentials.

Following a procedure used in Reference 3, one then transforms from P_z and z to γ and $\psi = (k_w + k_z)z - \omega t$ as the dependent variables, respectively, and from t to z as the independent variable. Next, one expands the resulting equations about the zero-order motion (i.e., the zero radiation field condition). This is facilitated by identifying the departure of electron energy from the resonant energy γ_o:

$$\delta\gamma_z = \gamma_z - \gamma_o \tag{6}$$

where γ_o is a solution to the transformed Hamilton's equation when A_s is set equal to zero. Averaging over one wiggler period, assuming that $a_w^2 << 1$ [where $a_w = eA_w/(mc^2)$ is the normalized wiggler strength parameter], and defining a normalized distance $\xi = z/(N_w \ell_w)$, one obtains the normalized equations of motion

$$\frac{d\psi}{d\xi} = \frac{\omega N_w \ell_w}{c(\gamma_o^2 - 1)^{3/2}}\,\delta\gamma \tag{7a}$$

$$\frac{d\delta\gamma}{d\xi} = -\frac{\omega}{c}\,\frac{a_w a_s N_w \ell_w}{(\gamma_o^2 - 1)^{1/2}}\sin\psi \tag{7b}$$

where N_w is the total number of periods in the undulator, and $a_s = \frac{e|A_s|}{mc^2}$ is the normalized radiation field amplitude. The final step is to define two generalized or "universal" normalized quantities:

$$\tilde{P} = \left[\frac{\omega}{c}\,\frac{N_w \ell_w}{(\gamma_o^2 - 1)^{3/2}}\right]\delta\gamma \tag{8a}$$

$$\tilde{A} = \left[\frac{\omega^2}{c^2}\,\frac{N_w^2 \ell_w^2}{(\gamma_o^2 - 1)^2}\right] a_w a_s \tag{8b}$$

Substituting Equations (8) into Equations (7) yields the universally normalized equations of motion:

$$\frac{d\psi}{d\xi} = \tilde{P} \tag{9a}$$

$$\frac{d\tilde{P}}{d\xi} = -\tilde{A}\sin\psi \tag{9b}$$

In Equations (9), we can identify $\tilde{P}$ as a generalized energy detuning parameter, and $\tilde{A}$ as a generalized beat wave potential amplitude.

The utility of expressing the pendulum equations in the form of Equations (9) is realized by computing the maximum generalized energy extraction for a beam of electrons having a uniform phase distribution, $\psi(\xi = 0) \in [0, 2\pi]$. This optimum energy extraction is computed as

$$\langle \Delta \tilde{P} \rangle_{\psi}\Big|_{max} = \tilde{P}(\xi=0) - \langle \tilde{P}(\xi=1) \rangle_{\psi} \tag{10}$$

where the brackets denote an average over the phase distribution. In Equation (10), (for a particular value of $\tilde{A}$) $\tilde{P}(0)$ is varied until $\langle \Delta\tilde{P} \rangle$ is maximized. We have calculated Equation (10) numerically using Equations (9). A plot of the universal optimized energy extraction versus the universal potential amplitude is shown as the solid line in Figure 3.

Equations (9) can also be used to obtain a small signal gain function formula by expanding quantities to second order in the (assumed) small quantity A. Following this procedures one obtains the universally normalized generalized small signal gain function

$$\tilde{G}(\tilde{P}) = \langle \Delta\tilde{P} \rangle A^2 = \frac{d}{d\tilde{P}}\left(\frac{\sin(\tilde{P}/2)}{\tilde{P}/2}\right)^2 \tag{11}$$

2.3. FEL Oscillator Equilibria Scaling Relations

To determine scaling relations for sheet-beam FEL oscillator equilibria, we identify the following radiation field definitions which are consistent with the equations derived above:

$$\underline{A}_s = [\hat{A}_s \cos(k_\perp y) e^{i(k_z z - \omega t)} - \hat{A}_s^* \cos(k_\perp y) e^{-i(k_z z - \omega t)}]\hat{e}_x, \tag{12a}$$

$$\underline{E}_s = -\frac{1}{c}\frac{\partial \underline{A}_s}{\partial t}, \tag{12b}$$

$$\underline{B}_s = \nabla \times \underline{A}_s. \tag{12c}$$

For the TE_{01} cavity mode we can now relate circulating cavity power P_{cav} and the normalized radiation vector potential a_s:

$$P_{cav} = \frac{k_z \omega}{4\pi} a_{rf} b_{rf} \left(\frac{mc^2}{e}\right)^2 a_s^2. \tag{13}$$

Substituting from Equation (8b) yields the following scaling relation for the cavity power:

$$P_{cav} = \left(\frac{k_z \omega}{4\pi}\right) a_{rf} b_{rf} \left(\frac{mc^2}{e}\right)^2 \left(\frac{c}{\omega}\right)^4 \frac{(\gamma_o^2 - 1)^4}{N_w^4 \ell_w^4 a_w^2} \tilde{A}^2. \tag{14}$$

Since k_z, ω, b_{rf}, γ_o, and ℓ_w must remain fixed for a fixed operating frequency, it is clear that

$$P_{cav} \propto \frac{a_{rf}}{N_w^4 a_w^2} \tilde{A}^2. \tag{15}$$

The efficiency of energy extraction η_e may be defined as

$$\eta_e \equiv \frac{\langle \Delta\gamma \rangle}{\gamma - 1} \equiv \frac{\gamma(\xi=0) - \langle \gamma(\xi=1) \rangle}{\gamma(\xi=0) - 1} \approx \frac{\delta\gamma(0) - \langle \delta\gamma(1) \rangle}{\gamma_o - 1}. \tag{16}$$

Using Equations (8a) and (10) we may obtain the scaling relation for efficiency

$$\eta_e = \left(\frac{c}{\omega}\right) \frac{(\gamma_o^2 - 1)^{3/2}}{(\gamma_o - 1)} \frac{\langle \Delta \tilde{P} \rangle}{N_w \ell_w} , \tag{17}$$

or

$$\eta_e \propto \frac{\langle \Delta \tilde{P} \rangle}{N_w} \tag{18}$$

for fixed FEL operating frequency.

An important quantity for FEL design is the thermal loading in the conducting cavity walls due to ohmic losses. Using formulas from Reference 4, time-averaged wall losses for the TE_{01} mode in units of power-per-unit-area can be written as

$$\hat{P}_{wall} \equiv \left\langle \frac{d^2 P_{wall}}{dxdz} \right\rangle \approx D \frac{(1 + R)}{a_{rf} b_{rf}} \frac{c}{k_z} \left(\frac{\pi}{b_{rf}}\right)^2 \frac{P_{cav}}{\sqrt{2\pi\sigma\omega}} \tag{19}$$

where R is the reflection coefficient at the cavity output, σ is the wall conductivity, and D is the duty factor for FEL operation. Using Equation (14) for P_{cav} yields the scaling for wall losses at fixed FEL frequency:

$$\hat{P}_{wall} \propto D \frac{(1 + R)}{N_w^4 a_w^2} \frac{\tilde{A}^2}{\sigma^{1/2}} \tag{20}$$

Clearly, wall losses become less of a concern for thermal stability of the cavity at low duty factors.

To complete the set of equations necessary for FEL design, an energy conservation relation is needed. A rigorous derivation of such a relation is possible by starting from the wave equation and expressing it in universally normalized quantities similar to the equations of motion above. For an oscillator with low gain per pass, however, we can assume that at equilibrium, the beat wave potential amplitude does not change appreciably from one end of the interaction region to the other (to lowest order). For these conditions we can identify a phenomenological power balance:

$$\eta_e = \frac{T_{eff} P_{cav}}{P_{beam}} \tag{21}$$

where T_{eff} is an effective "transmission" coefficient, representing all cavity losses (wall dissipation, extracted radiation power, and unintentional diffractive losses). Defining the beam power P_{beam} in terms of the beam current I_{beam}

$$P_{beam} = (\gamma_o - 1)\left(\frac{mc^2}{e}\right) I_{beam}, \tag{22}$$

we substitute Equation (17) for η_e to obtain an expression for the beam current:

$$I_{beam} = \left(\frac{e}{mc^2}\right)\left(\frac{\omega}{c}\right) \frac{N_w \ell_w}{(\gamma_o^2 - 1)^{3/2}} \frac{T_{eff} P_{cav}}{\langle \Delta \tilde{P} \rangle} . \tag{23}$$

Substituting from Equation (14) for the cavity power,

$$I_{beam} = \left(\frac{k_z \omega}{4\pi}\right) a_{rf} b_{rf} \left(\frac{mc^2}{e}\right)\left(\frac{c}{\omega}\right)^3 \frac{(\gamma_o^2 - 1)^{5/2}}{N_w^3 \ell_w^3 a_w^2} \frac{T_{eff} \tilde{A}^2}{\langle \Delta \tilde{P} \rangle} . \tag{24}$$

At low power, $\tilde{A}/\langle \Delta \tilde{P} \rangle$ can be identified as the inverse universal small signal gain function [cf. Equation (11)]. Moreover, we can take the limit as A approaches zero:

$$\tilde{G}_o \equiv \lim_{\tilde{A} \to 0} [\tilde{G}(\tilde{P})] \approx \frac{1}{15} \tag{25}$$

to obtain an expression for the start oscillation current

$$I_{start} = \left(\frac{k_z \omega}{4\pi}\right) a_{rf} b_{rf} \left(\frac{mc^2}{e}\right)\left(\frac{c}{\omega}\right)^3 \frac{(\gamma_o^2 - 1)^{5/2}}{N_w^3 \ell_w^3 a_w^2} \frac{T_{eff}}{\tilde{G}_o} \quad . \tag{26}$$

At this point it is convenient to define a ratio of beam current to start oscillation current:

$$\chi \equiv \frac{I_{beam}}{I_{start}} \quad . \tag{27}$$

With this definition we thus obtain a scaling relation for beam current

$$I_{beam} = \left(\frac{k_z \omega}{4\pi}\right) a_{rf} b_{rf} \left(\frac{mc^2}{e}\right)\left(\frac{c}{\omega}\right)^3 \frac{(\gamma_o^2 - 1)^{5/2}}{N_w^3 \ell_w^3 a_w^2} \frac{\chi T_{eff}}{\tilde{G}_o} \quad . \tag{28}$$

In addition, a comparison between Equations (24) and (28) reveals that for a fixed value of the current ratio χ,

$$\langle \Delta \tilde{P} \rangle = \frac{\tilde{G}_o}{\chi} \tilde{A}^2 \tag{29}$$

Several lines of constant χ have been plotted as the dashed curves in Figure 3.

2.4. FEL oscillator design procedure

If we symbolically denote the functional relationship between $\langle \Delta \tilde{P} \rangle$ and $\tilde{A}$ (i.e., the solid curve in Figure 3) as

$$\langle \Delta \tilde{P} \rangle = f_{optimum}(\tilde{A}) \tag{30}$$

then the general FEL oscillator design proceeds as follows. First, one chooses values for γ, ℓ_w, and b_{rf} which determine the FEL operating frequency. Second, one specifies a value for χ. Then simultaneous solution of Equations (29) and (30) yields the design values for the universally normalized quantities $\langle \Delta \tilde{P} \rangle$ and $\tilde{A}$. Next, one selects values for T_{eff}, a_{rf}, N_w, and a_w [$a_w \approx 0.93 \ell_w(cm) B_w(kG)$ where B_w is the peak on-axis wiggler field] and determines the beam current from Equation (28). At this point, the cavity power and the thermal wall loading can be calculated from Equations (23) and (19), respectively. The efficiency of energy extraction is determined from Equation (17) and the extracted radiation power can be estimated as

$$P_{out} \approx \eta_e \left(\frac{mc^2}{e}\right)(\gamma_o - 1) I_{beam} - 2\hat{P}_{wall} a_{rf} N_w \ell_w \tag{31}$$

If any of the calculated design quantities is unacceptable, revised designs can be determined by using the scaling relations and proportionalities described above.

Several comments regarding the validity of this design procedure are in order. First, it should be recognized that the design equations are based on oscillator configurations operating in a single (transverse and axial) TE_{01} mode, operating in a single electron (i.e., diffuse beam) limit, and having small values of T_{eff} (correlated with low gain per pass) as well as thin, stable sheet electron beams. Second, the quantitative designs discussed in this paper are restricted to a discussion of untapered wigglers. We have found that tapering may increase the theoretical efficiency η_e by up to factors of 2-3. The details of these calculations, however, will be discussed in future articles. Third, the formulas assume that the optimized energy extraction equilibrium is achievable, without addressing the issue of whether an oscillator will evolve to such equilibria from noise. To study this latter question, we have recently completed the development of a time-dependent, multiple (axial) mode, oscillator simulation model. Although the studies are still in progress, preliminary results indicate that choosing a value of $\chi \approx 4$ yields the fastest start-up for an oscillator with a stable single-mode equilibrium. Note from

Figure 3 that this value of χ also yields the highest achievable value of the universal energy extraction parameter $\langle\Delta\tilde{P}\rangle$. Hence, for short-pulse radar applications, an optimal choice for χ is approximately four, yielding design values for $\langle\Delta P\rangle$ and A of

$$\langle\Delta\tilde{P}\rangle_{radar} \approx 5.6,$$

$$\tilde{A}_{radar} \approx 18.$$

Other short period wiggler FEL applications may call for cw operation and/or lower power. In such cases, one may wish to choose lower values of χ.

2.5. Overall system efficiency

As mentioned earlier, the total system efficiency η_t can be enhanced by using a depressed collector to recover energy in the spent electron beam as shown in Figure 1. If the efficiency of this energy recovery is denoted by η_c then the total efficiency is

$$\eta_t = \frac{\eta_e \eta_w}{1 - \eta_c(1 - \eta_e)}, \tag{32}$$

where η_w is the circuit efficiency (taking wall losses into account) and we have neglected the current intercepted before reaching the collector.

For streaming electron beams found in devices such as traveling wave tubes and FEL's, recovery efficiency $\eta_c \approx 80\%$ is usually achievable with careful design, and $\eta_c = 97\%$ has been predicted as possible limit.[6] The major impact of this energy recovery is to minimize the value of ϕ_{LV} indicated in Figure 1. The time-averaged electrical power required to sustain FEL operation can be estimated to be

$$P_{elec} \approx \frac{P_{out}}{\eta_t} \approx \left(\frac{mc^2}{e}\right)(\gamma_o - 1)I_{beam}[(1 + \eta_e) - \eta_c], \tag{33}$$

where η_t is defined in Equation (32) and

$$\eta_w = \frac{P_{out}}{P_{out} + 2\hat{P}_{wall}\, a_{rf}\, N_w \ell_w}. \tag{34}$$

The value of ϕ_{LV} can be calculated as

$$\phi_{LV} = \phi_{HV}[(1 + \eta_e) - \eta_c]. \tag{35}$$

3. SHEET ELECTRON PROPAGATION EXPERIMENTS

As evident from Figure 1 and the discussion above, the feasibility of a short period wiggler FEL is highly dependent on the ability to stably propagate thin, wiggler-focused, sheet electron beams through narrow waveguide channels. A review of published literature on sheet electron beams indicates that the most stable configuration for sheet beam propagation involves wiggler-focusing without axial (magnetic) guide fields and conducting boundaries in close proximity to the beam.[5] We have recently completed experiments which support this hypothesis and will summarize the results as follows.

Wiggler focusing of relativistic sheet electron beams in narrow waveguide channels was observed for beams with energies of approximately 100 and 400 keV, using a wiggler having five periods and a period length of 1.0 cm. These sheet beams were approximately 30 mm wide by 1-3 mm thick and had currents between 15 and 30 A. The beams were generated using a pulse line accelerator, a field emission cathode, and a masking anode. For an on-axis wiggler field amplitude of approximately 1.6 kG, approximately 80% of the injected 40 keV beam current was recovered. This is compared with only 35% transmission of the unfocused 400 keV beam. Nearly 90% of the current in the 100 keV beam was transmitted at wiggler fields of 0.8 kG versus only 34% transmission without any wiggler focusing. The transmitted current data was in good agreement with theoretical predictions based on

confinement of single electron trajectories. In addition, no evidence of beam breakup or filamentation instabilities was observed. The experiments and analysis are described in detail in Reference 5. Planning for future experiments using longer wigglers is now in progress.

4. SUMMARY OF PROGRAM STATUS

We have developed the necessary theoretical tools to calculate oscillator equilibria for short period wiggler FELs employing sheet electron beams. Several examples are listed in Table I. For comparison, we have provided examples for a short-pulse 1 MW device, a cw 1 MW oscillator, and a low power cw source. Although not reviewed in this paper, we have also theoretically investigated the possibilities for an FEL amplifier in an optical klystron (OK) configuration.[7] These calculations indicate that gains of approximately 30 dB and efficiencies of a few percent are possible for FEL OK amplifiers operating at 150 to 300 GHz.

We have performed initial experiments which support the feasibility of propagating relativistic wiggler-focused sheet electron beams through narrow waveguide channels. These experiments used a five-period-long planar magnetic undulator having a 1.0 cm period length. Additional experiments are being planned using longer undulators with better field uniformity.

Designs of suitable interaction cavity configurations, both for laboratory experiments as well as eventual high power millimeter wave sources are in progress.

Finally, we are in the process of acquiring a 1 μs 450 kV thermionic Pierce electron gun for performing 150-300 GHz FEL oscillator experiments in our laboratory.

Table I. 300 GHz Short-Period Wiggler FEL Oscillator Designs (Untapered)

f_{res} (GHz)	298	298	298
P_{out} (peak, kW)	1100	1100	13
τ_{pulse} (μs)	1.0	CW	CW
Duty	0.001	1.0	1.0
ℓ_w (cm)	0.54	0.54	0.54
B_w (kG)	2.0	2.0	2.5
N_w	20	20	30
ϕ_{beam}, ϕ_{HV} (kV)	500	500	500
I_{beam} (A)	63	63	1.8
η_e (%)	4.2	4.2	1.5
a_{rf} (cm)	5.0	5.0	2.0
b_{rf} (cm)	0.22	0.22	0.22
P_{cav} (MW)	32.5 (peak)	32.5	0.33
P_{wall} (W/cm^2)	2 (avg.)	2000	64
P_{wall}, total (kW)	0.22 (avg.)	220	4.1
T_{eff} (%)	4.0	4.0	4.0
(I_{beam}/I_{start}), x	4.0	4.0	1.5
η_{w*} (%)	83	83	68
η_T (%)	17	17	4.7
ϕ_{LV} (kV)	120	120	108
P_{elec} (kW)	7.6 (avg.)	7600	194

* -- for a collector efficiency, η_c = 80%.

5. REFERENCES

1. V. L. Granatstein, T. M. Antonsen, Jr., J. H. Booske, W. W. Destler, P. E. Latham, B. Levush, I. D. Mayergoyz, D. J. Radack, Z. Segalov, and A. Serbeto, "Near-Millimeter Free Electron Lasers with Small Period Wigglers and Sheet Electron Beams," to be published in the Proceedings of the Ninth International Free Electron Laser Conference (Williamsburg, VA, 1987).
2. S. Ramo, J. R. Whinnery, and T. Van Duzer, Fields and Waves in Communication Electronics, (John Wiley and Sons, Inc., New York, 1965).
3. N. M. Kroll, P. L. Morton, and M. N. Rosenbluth, IEEE J. Quant. Elec. 17, 1436 (1981).
4. J. D. Jackson, Classical Electrodynamics, (John Wiley and Sons, New York, 1975).
5. J. H. Booske, W. W. Destler, Z. Segalov, D. J. Radack, E. T. Rosenbury, J. Rodgers, T. M. Antonsen, Jr., V. L. Granatstein, and I. D. Mayergoyz, "Propagation of Wiggler Focused Relativistic Sheet Electron Beams," submitted to J. Appl. Phys. (1987).
6. H. G. Kosmahl, Proc. IEEE 70, 1325 (1980).
7. M. C. Wang, V. L. Granatstein, and B. Levush, "The Gain and Efficiency Improvement of a Free Electron Laser by an Optical Klystron Configuration," accepted for publication in IEEE Trans. Plasma Sci. (1988).

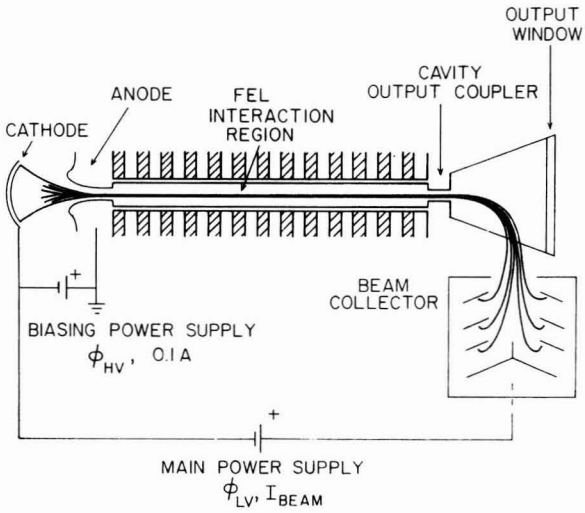

Figure 1. Cross-sectional schematic of a sheet beam FEL configuration. Beam voltage is determined by the high voltage bias ϕ_{HV} (~500 kV), while a depressed beam collector scheme reduces the voltage of the beam current supply to ϕ_{LV} (~100 kV).

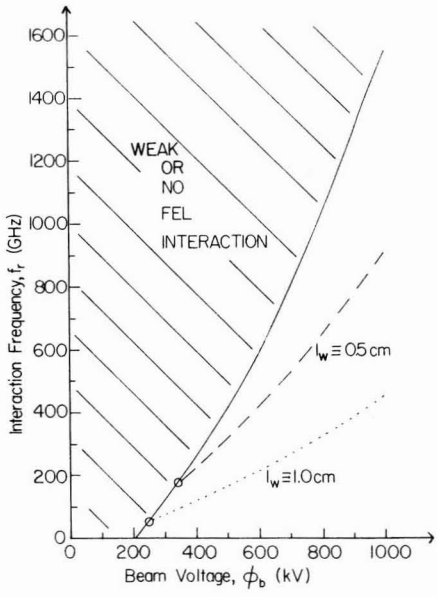

Figure 2. Accessible frequencies for short-period wiggler FEL operation. For this figure, a value of waveguide wall thickness t_{rf} = 0.25 mm was assumed.

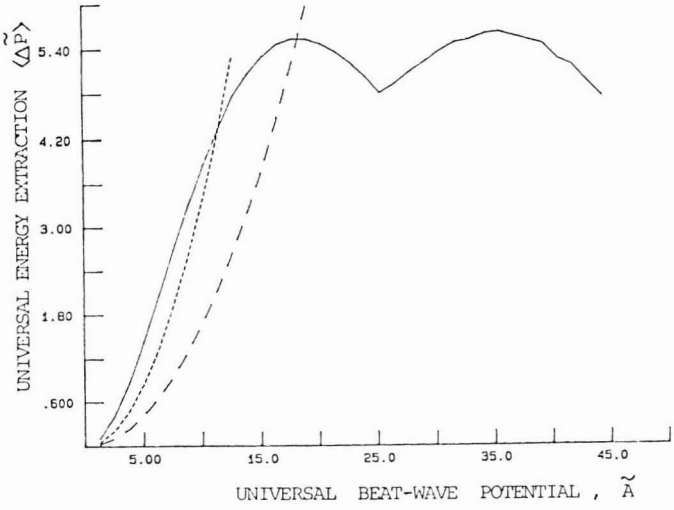

Figure 3. Optimized universal energy extraction curve for sheet beam FEL design (solid line). The other curves represent lines of constant values for the ratio of beam current to start oscillation current, χ [cf. Equation (20)]. In particular, plots for χ = 2 (dotted) and χ = 4 (dashed) are shown.